First Half-Reaction Mechanism of Nitric Oxide Synthase: The Role of Proton and Oxygen Coupled Electron Transfer in the Reaction by Quantum Mechanics/Molecular Mechanics

Kyung-Bin Cho, Maria Angels Carvajal,† and Sason Shaik*

Institute of Chemistry and The Lise Meitner-Minerva Center for Quantum Computational Chemistry, The Hebrew University of Jerusalem, 91904 Jerusalem, Israel

Received: August 15, 2008; Revised Manuscript Received: October 14, 2008

The first half-reaction of nitric oxide synthase (NOS) is investigated by means of quantum mechanical/molecular mechanical (QM/MM) calculations. An energetically feasible arginine hydroxylation path was found only when the iron−oxy complex accepted one proton from an external source. The so formed species has not been considered in heme chemistry; it is described as $Por^{+\bullet}Fe^{III}-OOH$ and is characterized by the same molecular constituency as the more known ferric−hydroperoxide species, compound 0, but has a cation-radical porphyrin moiety. The reaction itself is found to involve proton coupled electron transfer (PCET) and oxygen coupled electron transfer (OCET) steps en route to the formation of compound I and the ultimate monooxygenation of arginine. *The cofactor H_4B turns out to be a key player in the mechanism acting alternatively as an electron donor (when neutral) and an electron sink (when in its radical-cation state) and, thereby, providing the electron transfer component in the various coupled proton and oxygen transfer steps* (see Scheme 4). The various pieces of this mechanism account for many of the experimental observations, such as the following: (a) the origins of the second proton supplied to the heme, (b) the elusiveness of compound I, (c) the inactivity of peroxide-shunt pathways in NOS first half-reaction, (d) the inhibition of the H_4B analogue 4-amino-H_4B due to protonation at the N3 position, (e) the roles of Trp188 (iNOS numbering) and the crystal water at the active site (W115), and so on. Alternative mechanistic hypotheses are tested and excluded, and a new mechanism for the NOS second half-reaction is proposed.

Introduction

The physiological importance of nitric oxide (NO) radical as a signaling substance is well documented, and its usage is diverse covering the range of nervous, immune, and cardiovascular systems.[1−3] In this context, the activities of nitric oxide synthase (NOS) and its production of NO in vivo attract considerable interest. It is known that the reaction mechanism involves two half-reactions, shown in Scheme 1.[4−9] In the first half-reaction, L-arginine is converted to N^{ω}-hydroxyl-L-arginine (NHA) under consumption of O_2 and two reducing equivalents, the ultimate source of which can be traced to NADPH. In the second half-reaction, NHA is converted to L-citrulline and NO, consuming yet another molecule of O_2 and only one reducing equivalent (Scheme 1). NOS utilizes, in these reactions, tetrahydrobiopterin (H_4B) as a cofactor. While there exist many experimental results that contribute insight into the NOS reaction mechanism, a definite consensus mechanism is still missing. A major problem is the uncertainty about the active species that causes the hydroxylation of arginine and the subsequent decomposition of NHA, generally thought to be a high-valent unstable $Por^{+\bullet}FeO$ intermediate called compound I (cpd I); see below.

Since these mechanisms involve unstable and fleeting species, theoretical calculations can assist experiment by delineating viable reaction mechanisms. For instance, theory has been able to characterize the cpd I species, that is directly responsible for the oxygenation step in many heme systems but so far only been indirectly inferred experimentally in cytochrome P450 (P450). The valence electron configuration of cpd I has been shown to involve three unpaired electrons occupying two antibonding π^*-orbitals on FeO and an a_{2u} orbital (Figure 1) on the porphyrin, in two degenerate spin multiplicities (for a review, see ref 10). This and many other theoretical studies have made valuable contributions to the area of heme chemistry applicable not only to P450, but also to other enzymes such as chloroperoxidase[11] and heme oxygenase.[12] The methods and techniques used have so far been proven reliable (for a brief overview of this issue, see the Supporting Information). Accordingly, we continue here our use of these methods and present in this paper a quantum mechanical/molecular mechanical (QM/MM)[13,14] study to decipher the mechanism of the NOS first half-reaction. As shall be seen, the cofactor plays a major role as an electron shuttle that can donate an electron and accept it back at appropriate steps of the reaction mechanism, thereby assisting the generation of active species of the enzyme in situ in the process of monooxygenation of the arginine. In this Introduction, we outline some of the experiments done that are highly relevant and supports this mechanism, followed by a more comprehensive discussion later.

SCHEME 1: Two Half-Reactions of NOS

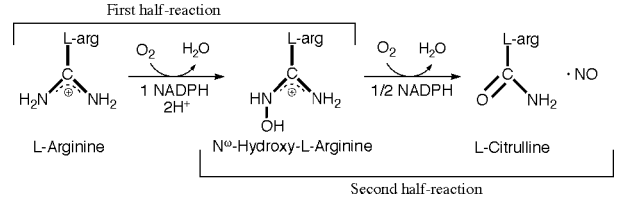

* E-mail: sason@yfaat.ch.huji.ac.il.
† Current address: Departament de Química Física i Inorgànica, Universitat Rovira i Virgili, Marcel·lí Domingo s/n − Campus Sescelades, 43007 Tarragona, Spain.

10.1021/jp8073199 CCC: $40.75
Published on Web 12/12/2008

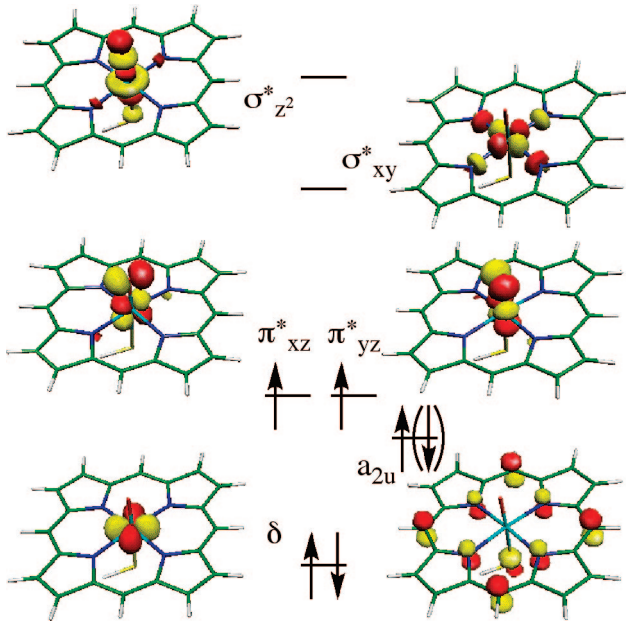

Figure 1. Electron valence orbitals involved in cpd I. The doublet and quartet species, the difference being in the spin type of the electron in the a_{2u} orbital, are usually degenerate in energy.

Considering that hydroxylating a substrate is a known feature of P450, it is generally thought that the NOS first half-reaction mechanism should follow the P450 paradigm, i.e. by formation of cpd I, which oxygenates the substrate, perhaps by a rebound mechanism. A proposed reaction mechanism representative of this line of thought is included in Scheme 2a, which is based on a recent resonance Raman spectroscopy results.[15] However, hard evidence for the existence of cpd I in NOS is still not established. Moreover, unlike in P450, the NOS first half-reaction does not take place using common peroxide-shunt pathway with oxygen surrogates such as iodosylbenzene (PhI═O), tert-butylhydroperoxide, cumene hydroperoxide, or H_2O_2.[16] It has therefore been proposed that cpd I is not reactive toward a fully protonated arginine, and as such cpd I may not be formed in the native system.[17] An alternative proposal was therefore recently suggested, as detailed in Scheme 2b.

Much of the NOS research is also directed toward elucidating the role of the cofactor H_4B. It was shown that H_4B-free enzyme could also support the first half-reaction, although with (much) lower efficiency.[18] This indicates that while H_4B may not be absolutely mandatory for the reaction, it is nevertheless an efficient cofactor, presumably playing a major role in the electron transfer reactions.[19] EPR results seem to verify the concluded hypothesis that H_4B is the second electron donor that acts in lieu of the reductase domain, due to its ability to donate the electron faster in a timely manner.[20−23] Although H_4B is known to have important properties in generating structural changes necessary for the reaction, it is nevertheless its function as an electron donor that is seen as the most important one.

Crystallographic studies do not reveal any structural differences between H_4B or its inactive analogue bound proteins,[24] supporting an additional role for H_4B besides electron donation, such as proton transfer from H_4B to the heme site,[25] although contradictory results and arguments against this exist.[24,26,27] Opinions seem to differ on whether the native H_4B radical occurs as a cation-radical species, or as a neutral radical after losing a proton; some results seem to support the neutral radical form,[28,29] while others support the cation-radical form.[25,27,30,31] *Thus, elucidation of the role played by H_4B in the catalytic hydroxylation of arginine is one of the major goals in the current study*.

In an attempt to isolate the intermediates in the NOS reaction mechanism, electron paramagnetic resonance (EPR) and electron−nuclear double resonance (ENDOR) experiments were conducted at cryogenic temperatures.[32] Unlike in other heme-enzymes, these experiments did not detect in NOS the ferric−hydroperoxide species, i.e. compound 0 (cpd 0). Instead, two new signals were observed with $g_1 - 2.54$ and $g_1 - 2.59$ EPR parameters, and the former signal converted to the latter with time. Due to the similarity of these signals with those from hydroxycamphor-heme complex in P450 as well as *N*-hydroxyguanidines-heme in 8-microperoxidase, the authors tentatively assigned the signals to an initial/equilibrated product complex where the product NHA is coordinated to heme. Other conclusions drawn in the cryo-annealing study are that the "first" proton needed for and entering the reaction (Scheme 1) may originate from elsewhere in the heme-pocket, while the "second" proton is delivered by the arginine. This is crucial mechanistic information, which as will be shown, is matched by the mechanism proposed herein.

Many studies have established that the bound L-arginine interacts with the ferrous-oxy (or, as we find in this study, ferric−superoxy) species.[15,33−36] Other potentially important species present in the active site is among else a water molecule, found in most crystal structures and is proposed to be a part of the proton shuttling mechanism from outside the active site.[32,37−39] Also, the active site include Trp188, a residue clearly hydrogen-bound to the heme cysteine sulfur which can affect the properties of the system, notably by the "push effect".[40,41] Trp188 mutants on nNOS are shown experimentally to affect the self-regulation step later on in the reaction cycle, by allowing faster release of NO from the Fe-NO moiety, thereby actually increasing the *overall* turnover rate,[42,43] but does not necessarily increase the rate of the NO formation step. In cytochrome c peroxidase (C*c*P) the presence of tryptophan leads to the formation of $Trp^{+\bullet}$ instead of the porphyrin cation radical when cpd I is formed.[44] The potential roles of crystal water and Trp188 are therefore examined in our study.

Taken together, these experimental results indicate an intricate interplay of different actors in the NOS reaction mechanism. In an attempt to unify these results, we have investigated the first half-reaction mechanism by means of QM/MM calculations using density functional theory (DFT)[45] as the QM method. We have in a previous study focused on potential roots of cpd I formation in NOS, assuming different protonation states of the iron−oxy species.[27] There, it was found that without an initial proton externally provided to the iron−oxy species, the conversion of $Fe^{II}-O_2$ ($Fe^{III}-O_2^-$) to cpd I (by deprotonating the substrate) was highly endothermic, and was not attended by the formation of the H_4B radical, as experimentally required. By contrast, providing one proton externally and starting from the singly protonated ferric−peroxy complex ($Por^{+\bullet}Fe^{III}-OOH$) was energetically more feasible and was attended by formation of a cation-radical species shared by H_4B and the deprotonated arginine substrate. Finally, providing two protons and commencing from the $Fe^{III}-HOOH$ complex, the formation of cpd I was exothermic (−25.7 kcal/mol), and was attended by the formation a cation-racial $H_4B^{+\bullet}$ species. Thus, our conclusion then was that "simultaneous" double protonation of Fe−OO species would be an attractive pathway for generating the NOS cpd I species, *but the singly protonated pathway was not altogether ruled out as a source of cpd I*. As we shall show in the present study, while all the previous conclusions remain intact, the double protonation path leads to a cpd I species that is highly stabilized and is unreactive toward arginine. In contrast,

SCHEME 2: Proposed Reaction Mechanisms in (a) Reference 15 and (b) Reference 17[a]

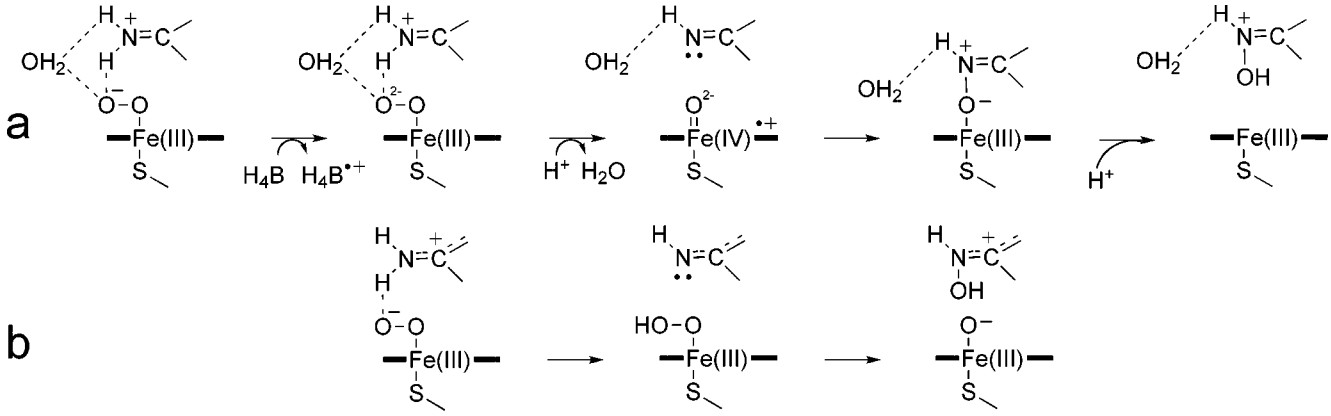

[a] The indicated electronic configurations were kept faithfully as presented in the references.

the single protonation mechanism generates a transient cpd I that is reactive and leads eventually to the formation of the hydroxylated arginine. In this mechanism, H_4B plays a role of an electron donor in a proton coupled electron transfer (PCET)[46] step that involves the arginine as the proton donor, and a fleeting cpd I species as the monooxygenating agent.

The paper is arranged in a hierarchical manner: It starts with a results section (section A) that describes a series of tests of many alternative mechanistic hypotheses for the first half-reaction, and concludes that the $Por^{+\bullet}Fe^{III}-OOH$ pathway is the most favorable one. Section B of the results further tests the role of environmental factors in the preferred mechanism. This is followed by the Discussion section that projects how the preferred mechanism accounts for the experimental data, and demonstrates the fleeting nature of cpd I. Scheme 4 and Figure 9 in the Discussion give succinct summaries of the so elucidated mechanism.

Methods

Setup. The setup of the system has been published earlier in detail, including the MM parameters.[27] In short, the A subunit of the PDB file 1NOD[47] was used with addition of missing residues and O_2, with two waters deleted at the active site to accommodate for O_2. The structure was then completed with hydrogens, and was repeatedly soaked/minimized/equilibrated in bulk water. The obtained structure was used for the Fe−OO calculations, while for the Fe−OOH, one proton was added to this structure and one additional cycle of soaking/minimization/equilibration was done. This structure was used in the same way as the startup for the Fe−HOOH structure. The residues in the MM region that were included in the geometry optimization are specified in the Supporting Information. As we pointed out before,[27] and in accord with experimental evidence,[37] the MD simulations show that sufficient number of water molecules pass through the active site and may therefore shuttle protons to generate these protonated species.

QM/MM. Calculations were done using ChemShell 3.1b1[48] combining the calculations of Turbomole 5.71[49] on the QM region and DL_POLY[48] (as built-in in ChemShell) on the MM region. Hybrid DFT[45] was used for the QM part, using the B3LYP functional.[50−53] The reliability of B3LYP functional in heme systems has been discussed amply elsewhere and is summarized in the Supporting Information. Basis sets employed were LACVP for geometry optimization, and LACV3P*+ on the optimized structure to obtain accurate energies, Mulliken spin and charge distributions. These single point calculations

SCHEME 3: Schematic View of the QM Region Used in the Calculations[a]

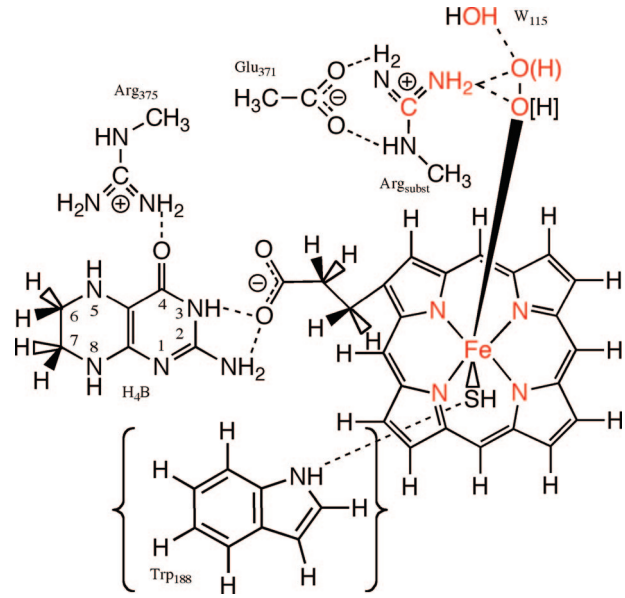

[a] Numberings as used in the text are marked for H_4B. Protons in brackets and parenthesis may or may not be included depending on the pathway studied. Trp188 was included only when mentioned explicitly in the text. The 14 core atoms used in transition state searches and frequency calculations are marked in red.

were done using Jaguar 5.5[54] and a special ChemShell interface written in our laboratory. Also, some studies suggest that a 15% Hartree−Fock exchange instead of the standard 20% in B3LYP may be more accurate in transition metal containing systems (termed B3LYP*).[55,56] Therefore, for the key transition states in the present study, we have also calculated the B3LYP* single-point energies with LACV3P*+ basis set. For the MM part, standard CHARMM22[57] parameters were used in combination with own developed parameters for the heme moiety and H_4B as previously described.[27] The treatment of the link atoms between the QM and MM regions followed the charge-shift scheme.[58] For transition state search and frequency calculations, the Hessian was calculated numerically as defined in ChemShell for designated 14 core atoms[13] (hereafter referred to as "core atoms", marked in Scheme 3) in the QM/MM setting. The use of core atoms is a common practice in QM/MM since a full frequency calculation is not feasible. Thus, while the Hessian does not contain the dimensions of the atoms not included in the core region, it does contain the influences of these atoms.

Hence in the case of transition states, enlarging the Hessian dimensions will, if at all, only lead to an energetically lower state, thereby not affecting the proposed mechanism. Changing the core could affect the thermal contributions to the energy (zero-point vibrational energy, enthalpy and entropy), but this is not expected to change the *relative* energies in a significant way due to expected cancelations of contributions from outside the core region.

QM Region Used. The QM region used in this study corresponds to what was used in our previous study, but is now extended (and optimized) with additional CH_3 on Arg375, the methyl-carboxylate group of Glu371, and a crystal water molecule present in the pocket (Scheme 3). The technical reasons for these extensions and their consequences are given in the Supporting Information. It should be pointed out that adding these groups in the QM region are "improvements" rather than new "inclusions"; the effects of these additional groups were already present before but only in the less accurate form of MM charges, which influenced somewhat the radical concentration on H_4B. A few other QM regions than the one shown in Scheme 3 were also calculated and described where appropriate in this study.

The energy values presented here are by default the values obtained with LACV3P*+ basis set, not including any thermal effects, unless otherwise stated. This is because frequency calculations were done only when necessary; hence the LACV3P*+ values are the ones that are the most accurate uniform values available which can be compared directly between *all* the structures in this study. Whenever necessary however, thermal effects will be discussed, but one should be aware that the addition of these thermal effects gives the free energy of the QM system only, embedded in the MM charges (Table S3 in the Supporting Information). This is not a full free energy, which in turn requires extensive sampling of the conformational space during the reaction,[59] something we cannot do here.

Spin State. Our calculations focus in this study on the singlet (multiplicity =1) spin state, as this is the energetically lowest state in general. The reasoning behind this is first to avoid time-consuming repetitive calculations on the different spin multiplicities. Second, we know by experience that the other multiplicities are energetically close, and hence, while the reactions may follow two/multistate reactivity (TSR/MSR),[10] this will not affect the efficiency of the mechanism proposed here. Nevertheless, to ascertain the role of TSR/MSR, we do discuss possible alternative multiplicities for key states.

Results

A. Testing the Alternative Mechanistic Hypotheses for the Arginine Hydroxylation Process. The computational approach in the present study is based on the same logic applied previously.[27] Thus, the first half-reaction is explored for three protonation states of the heme at the beginning of the reaction: no additional protons (i.e., Fe−OO), one (Fe−OOH), or two (Fe−HOOH). Subsequently, the reactivity of each species in hydroxylating arginine is assessed in order to find the most likely mechanism. Our results are therefore presented below in three subsections differentiated by the different protonation states, and then an additional section describing calculations done with different variations in the enzymatic environment and the cofactor. Table 1 summarizes relative energies and other features of key species that are discussed below.

A.1. Unprotonated $Fe^{III}-OO^-$ Ferric−Oxy Pathway. Our previous results already excluded the reaction commencing with $Fe^{III}-OO^-$ ($Fe^{III}-OO^{-\bullet}$ is a more precise description, where Fe^{III} and $O_2^{-\bullet}$ are coupled to a singlet state; however, we are keeping the $Fe^{III}-OO^-$ notation). This exclusion was based on the high endothermicity in forming cpd I, and the failure to generate the experimentally observed radical on H_4B. Using the enlarged QM region in this study, this could again be verified; no spin was found on H_4B and cpd I was 26.1 kcal/mol above the starting point. To counter arguments that the NOS first half-reaction will not natively generate cpd I, we have tried the alternative pathway suggested[17] in Scheme 2b where the iron−oxy species itself performs the substrate hydroxylating reaction. The first step of this reaction involves abstraction of one of the NH-protons from the substrate. All attempts to transfer the proton to the $Fe^{III}-OO^-$ moiety resulted in the proton instantly returning to its origins, the N atom of the substrate. To avoid this collapse, the only way to generate a "Fe−OOH" species was to manually redirect the OH direction away from the substrate, pointing toward one of the heme nitrogen atoms instead (structure **0a**, Figure 2). The energy of such a reaction however, was calculated to be endothermic by 35.9 kcal/mol. With such a high endothermicity (and presumably even a higher transition state going to/from this intermediate), we deemed this process to be impossible.

To further ascertain the putative role of $Fe^{III}-OO^-$ species, we also calculated a ferric−peroxy $Fe^{III}-OO^{2-}$ complex, where an extra electron was added to the system (structure **0b**, Figure 2). This would for instance mimic the structure used in the EPR/ENDOR experiments[32] where an extra electron was "forced" into the system by means of γ-irradiation at cryogenic temperatures. This extra charge placed on the O_2 moiety was enough to partially abstract the substrate proton, where the optimized structure showed this proton to be hydrogen-bonded, only 1.32 Å away, to the outer oxygen of $Fe^{III}-OO^{2-}$, with a long bond length to the substrate N of 1.18 Å. Hence, if a peroxide species $Fe^{III}-OO^{2-}$ can be formed, it is plausible that a proton abstraction from the substrate can readily occur, driving the reaction forward to cpd 0. However, in the cryogenic experiments, a known inactive H_4B analogue (4-amino-H_4B) was used as a cofactor. At the same time, our calculations show that the peroxide $Fe^{III}-OO^{2-}$ species does not form in the native system, since the iron−oxy complex cannot abstract an electron from H_4B. Therefore, our calculations do not support the pathway described in Scheme 2b.

A.2. Doubly Protonated Pathway. Starting with a doubly protonated structure $Fe^{III}-HOOH$, the formation of cpd I is found here to be exothermic by 24.9 kcal/mol, thus confirming

TABLE 1: Mulliken Spin Density Distribution for the Key Species Studied in This Paper and Their Relative Energies

	Fe	O_{inner}	SH	Por	subs	H_4B	HO_{outer}	rest	ΔE^a
0a	1.17	−0.40	−0.07	−0.10	−0.57	0.00	−0.03	0.00	**35.9**[b]
0b	0.96	0.13	−0.01	−0.08	0.00[c]	0.00	0.00[d]	0.00	
0c	1.93	0.36[e]	−0.22	−1.06	−0.01	−1.00	0.01[f]	0.00	**18.8**[g]
0d	1.25	0.50	−0.25	−0.63	0.14[c]	−1.00	0.00	0.00	**44.3**[g]
1a	1.12	0.01	−0.10	−0.71	0.00[c]	−0.31	−0.01	0.00	**0.0**
1b	1.09	0.03	−0.09	−0.67	0.00[c]	−0.35	−0.01	0.00	**0.4**
TS1	1.51	0.57	−0.29	−0.71	0.00[c]	−0.45	−0.65	0.00	**19.7**
2	1.44	0.74	−0.26	−0.91	0.00[c]	−0.47	−0.54	0.00	**17.7**
TS2	1.36	0.80	−0.26	−0.97	−0.10	−0.81	−0.01[f]	0.00	**19.1**
3	1.40	0.77	−0.25	−0.93	−0.23	−0.76	0.00[f]	0.00	**9.2**
TS3	1.64	0.19	−0.19	−0.62	−0.58	−0.44	0.00[f]	0.00	**23.1**
4	1.16	0.00	−0.12	−0.58	−0.02	−0.45	0.00[f]	0.00	**−11.9**
5 septet	4.15		0.37	0.52	−0.01[h]	0.96	0.00[f]	−0.00	

[a] B3LYP/LACV3P*+/MM//B3LYP/LACVP/MM energies relative to **1a** in kilocalories per mole. [b] Relative to Fe−OO. [c] Protonated substrate. [d] O_{outer}. [e] HO_{inner}. [f] H_2O_{outer}. [g] Relative to cpd I. [h] Hydroxylated substrate.

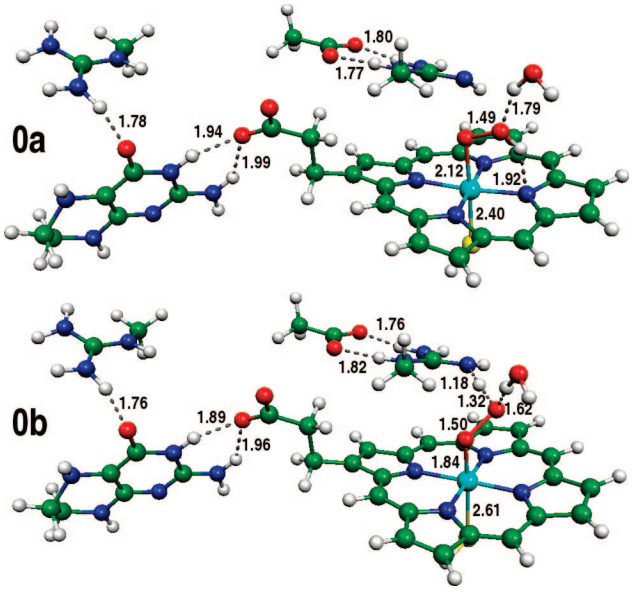

Figure 2. Two possible structures starting from the $Fe^{III}-OO^{-}$ species: the hydrogen abstracted structure (**0a**) and the electron reduced $Fe^{III}-OO^{2-}$ species (**0b**). Hydrogen bonds as well as O−O, Fe−O, and S−Fe distances are given in angstroms.

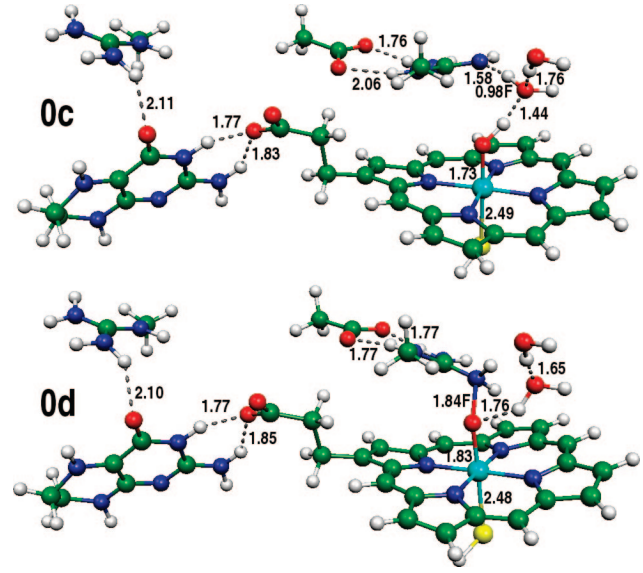

Figure 3. Optimized structures **0c** and **0d** along the rebound mechanism of cpd I nascent from the Fe−HOOH pathway. Frozen distances during optimizations are marked with "F". Hydrogen bonds as well as H−OH (**0c**), N−O (**0d**), Fe−O, and S−Fe distances are given in angstroms.

our previous results.[27] Therefore, we have performed an extensive search for a pathway whereby this cpd I could possibly hydroxylate the substrate. These calculations involved QM models of different sizes, cpd I interaction with virtually all atoms on the substrate and using different structures from long MD dynamics. The results were the same: the so formed cpd I did not lead to any viable pathway. To exemplify this conclusion, we present below two of the more credible pathways out of many trials.

In the related enzyme P450, the cpd I species abstracts a hydrogen atom from an R−H substrate, thereby forming an iron hydroxo/radical intermediate ($Fe^{IV}-OH/R\bullet$), which then undergoes rebound to form a hydroxylated substrate. To estimate the barrier for hydrogen abstraction, we scanned the ArgN-H-(OH_2)OFe coordinate, and found that the energy does not reach any intermediate, but keeps rising. To nevertheless obtain an energy value, we froze the OH distance of water to 0.98 Å and relaxed everything else (**0c**, Figure 3). This resulted in a strong N−H hydrogen bond of 1.58 Å and an endothermicity of 18.8 kcal/mol (compared to cpd I), a value that gets higher as Fe−OH has to break this strong hydrogen bond and reposition itself to reach the substrate in the putative rebound reaction (an FeO−N distance of 3.62 Å). Analysis of the spin density features indicates that in fact the $Fe^{IV}-OH$ complex is not actually formed, as the reaction turned out to be a proton transfer (hence the resulting $Por^{+\bullet}Fe^{IV}OH$ species was a protonated cpd I). On the basis of this and various model trials that indicated a true barrier upward 30 kcal/mol, we find it unlikely that the reaction occurs along this pathway.

Similarly we tried a direct *N*-oxygenating step, which resulted in an approximate transition state, i.e. the highest point of the scan, being 44.3 kcal/mol higher than the cpd I state (**0d**, Figure 3).

Our conclusion is therefore that while the doubly protonated path can easily form cpd I (ignoring any uncoupling of H_2O_2), the so resulting species is too stable to react with a fully protonated substrate arginine. *Thus, cpd I formation via the double protonation path is a dead-end species.*

Other Potential Reactions via the Double Protonation Path. As was already shown,[27] and reconfirmed here, the septet is the lowest spin state for the $Fe^{III}-HOOH$ complex that initially forms via a putative double protonation path. In turn, the septet state possesses an Fe−O bond length of 2.99 Å, i.e. it is essentially broken (Figure S34 in the Supporting Information). As such, very likely, this initial complex will undergo preferentially H_2O_2 uncoupling (see the Discussion) and will generate only small yields of cpd I, via the lower spin states.

However, the double protonation route has relevance for the so-called peroxide shunt pathways, where oxygen surrogates such as H_2O_2 or PhI═O are used to generate a competent cpd I that leads to monooxygenation in P450, but these surrogates fail to do so in NOS.[16] In order to investigate this path as well, the structures **0c** and **0d** of Figure 3 were reoptimized, but now with one more electron that converts $H_4B^{+\bullet}$ to H_4B, which is the right total charge needed to simulate the H_2O_2 binding to Fe^{III} and subsequent cpd I formation. Also here, the structure corresponding to **0c** had the OH distance frozen to 0.98 Å, resulting in a N−H distance of 1.59 Å (Figure S38 in the Supporting Information). The endothermicity for this structure was at 22.1 kcal/mol above the corresponding cpd I structure. Again, a substantially higher actual barrier is expected here. For the direct oxygenation structure (corresponding to **0d**), a maximum point in the scan was reached at the O−N distance of 1.85 Å, at 35.1 kcal/mol above cpd I (Figure S39 in the Supporting Information). *Thus, these results further show that cpd I cannot interact with a fully protonated arginine substrate.*

A.3. Monoprotonated Ferric−Superoxy Pathway. $Por^{+\bullet}Fe^{III}-OOH$ Species. Single protonation of $PorFe^{III}-OO^{-}$ leads to the $Por^{+\bullet}Fe^{III}-OOH$ species, as the OOH moiety abstracts an electron from the porphyrin to form the hydroperoxo species. On the basis of the moderate endothermicity of cpd I formation via this species (12.4 kcal/mol),[27] we considered this to be "a borderline case" for cpd I formation. However, as we show below, the subsequent kinetic barrier for this species to hydroxylate arginine is rather low, thus making this pathway a prime candidate for the first half-reaction. The relative energies and spin densities of the species that occur along the hydroxylation path, starting from $Por^{+\bullet}Fe^{III}-OOH$ (**1**), can be found in Table 1. The intermediates and transition states presented below

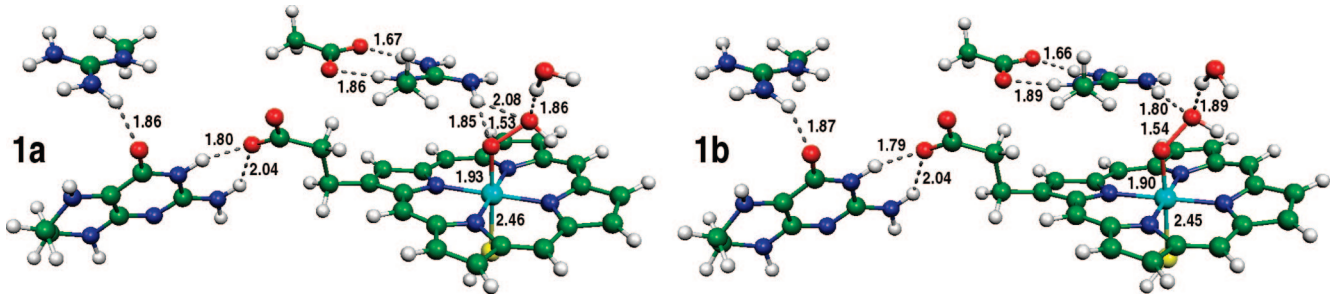

Figure 4. Two starting structures **1a** and **1b** of $Por^{+\bullet}Fe^{III}-OOH$. Hydrogen bonds as well as O−O, Fe−O, and S−Fe distances are given in angstroms.

essentially follows the reaction proposed in Scheme 2a, but differences exists and are addressed more thoroughly in the Discussion.

Figure 4 shows two $Por^{+\bullet}Fe^{III}-OOH$ species that are obtained by adding a proton to the $PorFe^{III}-OO^{-}$ complex and will constitute our starting points. **1a** corresponds to the structure we published earlier,[27] with the substrate forming a hydrogen bond to the proximal oxygen of Fe−OOH. Despite the Fe−OOH constitution, *this is not a cpd 0 structure* as the species observed for instance in P450. Here, the structure is one electron deficient compared to cpd 0; this deficiency is manifested by a singly occupied a_{2u} orbital on the heme (Figure 1) in addition to the d_{yz} orbital on the iron, thus corresponding to $Por^{+\bullet}Fe^{III}-OOH$. As such, this species is related to cpd I ($Por^{+\bullet}Fe^{IV}=O$) with a hydroxyl radical added to the Fe=O moiety.

The generation of the $Por^{+\bullet}Fe^{III}-OOH$ species is now attended by small spin development on H_4B (−0.31, Table 1). This spin density together with the spin on porphyrin sum up to virtually 1; thus the a_{2u} and H_4B valence orbitals interact and form a delocalized singly occupied orbital representing a partial electron donation from H_4B to porphyrin via the propionate side chain of the heme (Figure 4).

Upon hydrogen bonding reorganization, **1a** is converted to **1b** (Figure 4), where the substrate arginine is hydrogen bonded only with the distal oxygen of the FeO−O moiety. The energy of this structure is slightly higher than **1a** (0.4 kcal/mol), mostly because of differences in the less accurate MM energy contributions (Table S3 in the Supporting Information). The electron configuration is basically the same as **1a**, with a slightly larger spin on H_4B (−0.35 vis-à-vis −0.31, Table 1).

Because this is our starting point, finding the energetically lowest structure here is particularly important, as our barriers further along the reaction will be calculated relative to this state. We therefore verified that the triplet state is indeed higher in energy for the current model; the triplet structure corresponding to **1a** was 0.65 kcal/mol higher. Also here, the spin was delocalized with 0.33 in spin distribution on H_4B (Figure S5 in the Supporting Information), showing that the spin delocalization is not an artifact of antiparallel spin coupling sometimes seen in unrestricted singlet systems.

O−O Bond Breaking Step. The first step of the reaction is the O−O bond breakage in $Por^{+\bullet}Fe^{III}-OOH$. The energy value found for this transition state **TS1** is 19.7 kcal/mol (17.9 kcal/mol with thermal effects). Using B3LYP*, the corresponding value is 16.2 kcal/mol (14.4 kcal/mol with thermal factors), i.e. 3.5 kcal/mol lower than the B3LYP datum. **TS1** is quite complex, involving not only the O−O bond break, but also a reorientation of the free OH species that is formed. This reorientation is necessary since a hydrogen bond is formed to the cpd I oxygen (Figure 5), stabilizing the structure and preventing the reaction to go back to **1**.

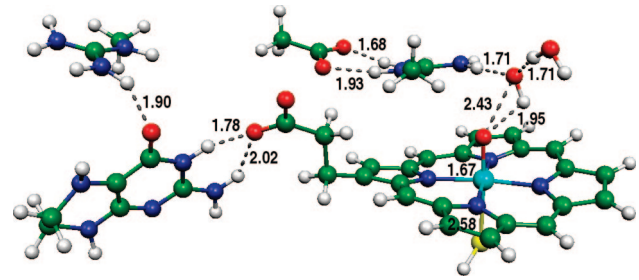

Figure 5. O−O bond breaking transition state, **TS1**, nascent from $Por^{+\bullet}Fe^{III}-OOH$ (**1**). Hydrogen bonds as well as Fe−O and S−Fe distances are given in angstroms.

The O−O breakage step results in the intermediate **2** (Figure S7 in the Supporting Information), that involves cpd I and OH, and where the OH species is clawed in space by hydrogen bonds to both the substrate and the crystal water. Energetically, this structure is at 17.7 kcal/mol above the starting point (13.5 including thermal effects).

In principle, since the starting structure is $Por^{+\bullet}Fe^{III}-OOH$, the departure of an OH radical species will lead to the formation of cpd I. A closer look at the spin distribution shows that the OH species in fact is half-radical and half an ion (−0.54, Table 1), since it accepts half an electron from H_4B. This half-radical/half an ion hybrid character of OH facilitates the next step; the proton abstraction from the substrate.

Arginine Deprotonation Step by PCET. In the next step of the reaction, the substrate gets deprotonated by the OH radical/anion through the transition state **TS2** to form the intermediate **3**. Remarkably, the spin distribution at **TS2** (Figure 6) indicates that the missing negative charge of the hybrid OH species is now completed by means of a proton coupled electron transfer (PCET). Thus, en route to becoming a water molecule, the OH species draws a full electron from H_4B, becomes OH^{-} and at the same time undergoes protonation by the substrate. The substrate itself develops only a minor amount of spin (−0.10), which is changed slightly to −0.23 at the following intermediate state **3** (Figure S9 in the Supporting Information) and is thus mostly in its neutral form. On the basis of this, we propose that the primary role of the H_4B electron transfer is *to provide one electron and thereby allow a deprotonation of the substrate arginine, rather than the energetically costly hydrogen atom abstraction*. This deprotonation process leads to a neutral arginine with a C=NH double bond. Except for geometrical differences around the N−H−O bonds, no other notable differences are seen between structures **TS2** and **3**. The energies are now at 19.1 and 9.2 kcal/mol (10.1 and 7.8 with thermal effects), respectively. The triplet state of **3** (with a quartet state heme, Figure S10 in the Supporting Information) is calculated to be at 9.6 kcal/mol, in line with the known degeneracy of the two lowest spin states of cpd I.[10] The quintet state, i.e. heme

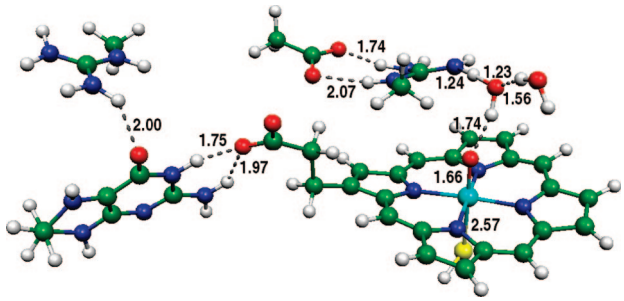

Figure 6. Substrate deprotonation transition state **TS2**, nascent from cpd I + OH• (**2**) and leading to **3** (shown in Figure S9 in the Supporting Information). Hydrogen bonds as well as N−H−O, Fe−O, and S−Fe distances are given in angstroms.

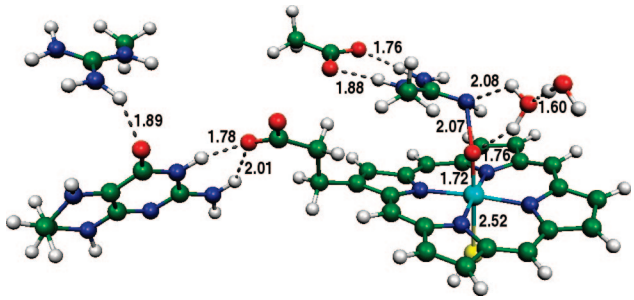

Figure 7. N-oxygenation transition state **TS3**, leading to **4**, which involves FeO−N formation and occurring by an OCET mechanism. Hydrogen bonds and N−O, Fe−O, and S−Fe distances are in angstroms.

quartet together with a parallel spin on H_4B, is like the singlet also at 9.2 kcal/mol with a similar spin distribution, showing once again that the spin delocalization is not an artifact of antiparallel coupling of the spins (Figure S11 in the Supporting Information).

Arginine Oxygenation Step. The final step starts from **3**, which upon oxygenation of the deprotonated arginine via **TS3** (Figure 7) yields the intermediate **4** (Figure S13 in the Supporting Information). Thus, starting with **3**, we have a neutral arginine with a C═NH double bond just above the oxo group of cpd I. As expected, much as in olefin epoxidation by cpd I,[60] cpd I attacks the double bond and forms an FeO—N bond. Had it not been for the $H_4B^{+\bullet}$, the C═NH bond activation would have generated a radical carbon atom adjacent to the NH moiety. However, in the presence of the $H_4B^{+\bullet}$ radical, the electron density flows back partially to $H_4B^{+\bullet}$ and partially to the porphyrin. The result is an intermediate product **4** with virtually a carbocation center on the carbon atom of arginine (Table 1). Hence, we see in effect an oxygen coupled electron transfer (OCET). The barrier for FeO—N bond formation to the arginine is 23.1 kcal/mol (B3LYP*: 18.8 kcal/mol); with thermal effects this barrier is only 16.4 kcal/mol.

Product (NHA) Forming Step. The intermediate structure **4** lies at −11.9 kcal/mol (−15.9 with thermal effects). It possesses an oxygenated arginine ligated to Fe, but is still lacking a proton on the oxygen to form the final hydroxylated arginine (NHA in Scheme 1). While we cannot estimate the energetic cost of bringing in a proton from outside to form NHA, the short hydrogen bonds (1.60−1.65Å, Figure S13 in the Supporting Information) through the both waters present in the QM region are suggestive of a possible protonation pathway through a Grotthaus-type mechanism. The amount of spin on H_4B is just below half an electron, but is expected to supply the remaining half when the additional proton is provided; hence another PCET process (Table 1).

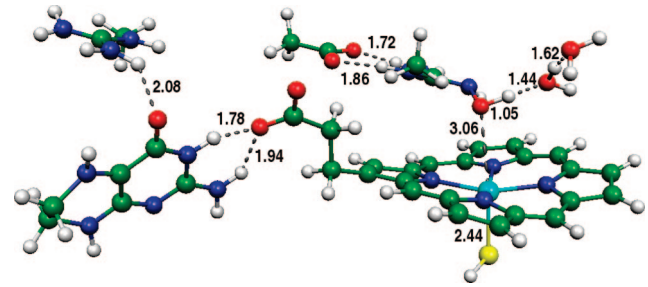

Figure 8. Final hydroxylated arginine product structure **5** (in the septet state), obtained by external protonation and electron transfer from H_4B. Hydrogen bonds as well as NO−H, Fe−O, and S−Fe distances are given in angstroms.

To test our deduction, we placed an extra proton on the crystal water in **4**, thereby forming H_3O^+. The expectation was that the subsequent optimization would automatically shuttle a proton through the water chain to protonate the ArgNO moiety, thereby simulating the Grotthaus mechanism. This was indeed exactly what happened, and the end structure **5** involves a ferric complex of NHA with a long Fe···O bond (Figure S14 in the Supporting Information). Thus, these results show the feasibility of the Grotthaus mechanism occurring in the current system. The ground-state structure (Figure 8) is a septet state where the a_{2u} valence orbital on porphyrin is now doubly occupied due to an electron transfer from H_4B, which now indeed has a full spin. The radical on $H_4B^{+\bullet}$ will henceforth remain until the reductase domain supplies the replacement electron needed to start the second half-reaction.

B. Calculations of Surrounding Factors Potentially Affecting the $Por^{+\bullet}Fe^{III}$−OOH Pathway. ***Further Elucidation of the Role of H_4B.*** To elucidate the role of H_4B in the $Por^{+\bullet}Fe^{III}$−OOH pathway, we carried out calculations with a smaller QM region, where H_4B, Arg357, and the propionate arm were put in the MM region instead. This created an interesting situation; while keeping the structural and long-range electrostatic effects of H_4B, we exclude it from interacting directly with the electronic configuration of the system. Experimentally, this would correspond to using an inactive H_4B analogue (here this is done by using H_4B itself but as an MM element). A reasonable assumption is then that the structures around the cpd I formation step would be most affected by this, since this is where H_4B participates electronically in the PCET to facilitate the cleavage of the O−O bond. The energetic effect is indeed dramatic for the barrier at **TS2** (obtained by keeping the core atoms frozen from the larger model) *raising the barrier from 19.1 to 27.7 kcal/mol*. Spin distribution at **3** reveals that in this case, the electron needed for the water formation comes partly from the substrate (which now has a spin of −0.54), but also partly from the a_{1u} orbital of porphyrin (Figure S22 in the Supporting Information). Thus, the porphyrin orbitals a_{1u} and a_{2u} together with the σ-orbital on sulfur exhibits a total of 1.63 in spin at structure **3**. With H_4B, **3** is at 9.2 kcal/mol above the starting point, without it, the energy is at 17.2 kcal/mol. **TS1** and **TS3** however are only marginally affected by this, as the energies are at 22.1 and 24.3 kcal/mol (compared to 19.7 and 23.1), respectively, indeed indicating that most important role for H_4B seems to be the facilitation of substrate deprotonation by the electron transfer to the incipient OH-radical species.

Replacing H_4B with the inactive analogue 4-amino-H_4B further elucidates the role of H_4B. The starting structure **1a** with this analogue instead (Figure S27 in the Supporting Information) produced −0.28 in spin on 4-amino-H_4B, almost the same as in the native system (−0.31). Also, the energies were hardly

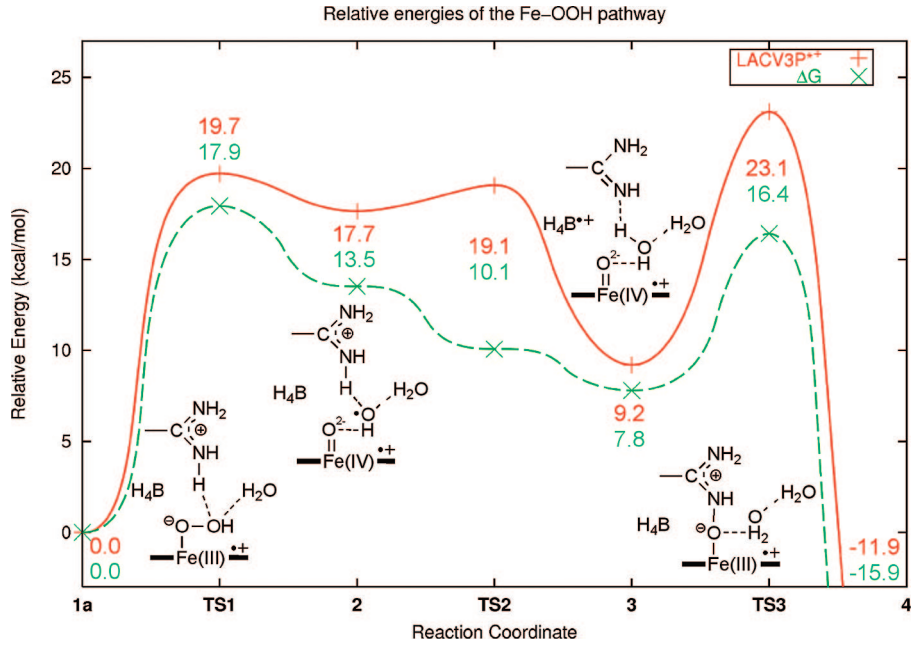

Figure 9. Energetics of the first half-reaction nascent from the $Por^{+\bullet}Fe^{III}$—OOH pathway. The red solid curve shows the energies calculated by the LACV3P*+ basis set, while the green dashed curve also includes thermal effects (i.e., Gibbs free energy of the QM-only subsystem).

affected; the **TS1**, **TS2** and **TS3** energies obtained with core atoms frozen from the H_4B structure were 19.5, 19.7 and 23.3 kcal/mol, respectively. This is to be compared to 19.7, 19.1, and 23.1 kcal/mol in the native system. Similar results were gained using the 4-imino tautamer of H_4B (where N3 is protonated instead, data not shown). Since 4-amino-H_4B is a better proton acceptor than H_4B, we looked at the impact of protonation of the cofactor analog. Thus, *using an N3 protonated 4-amino-H_5B^+ cofactor, the energy at* **TS2** *is found to be at 29.75 kcal/mol, and no spin is developed at any time on 4-amino-H_5B^+* (Figures S31 and S32 in the Supporting Information). We can therefore conclude that if 4-amino-H_4B would bind to the active site protonated at the N3 position (i.e., as 4-amino-H_5B^+), as indeed suggested by the crystallographic data,[24] the reaction would be inhibited.

Role of Trp188. To investigate its putative effect in NOS,[40−44] we used an enlarged QM region, where the indole ring of Trp188 is included. The results show that for structure **3** (Figure S25 in the Supporting Information), Trp188 develops some spin, although only by −0.08. Also, it is found that the difference in the relative energy was minor (8.4 vs 9.2 kcal/mol before). To check the effect on **TS3**, we reoptimized the **TS3** structure including the indole ring (Figure S26 in the Supporting Information), but with the core atoms frozen in their positions. Also here the effects were rather minor, with the energy at 22.2 (vs 23.1) kcal/mol, and no spin on Trp188. Hence, our conclusion is that while Trp188 seems to influence the electronic structure and lower the barrier in this part of the reaction, the effects are rather small. These calculations do not address the importance of Trp188 structural or pure electrostatic effects (in which the "push effect" could be part of), as they are still present when Trp188 is in the MM region. To completely describe the role of Trp188 in depth would require a full in silico Trp188 mutation calculations, which is out of scope for this study.

Role of Crystal Water W115. One might suspect that this water molecule could also have a role in facilitating the FeO−OH bond breakage via **TS1**. To test this, the crystal water was removed, and structures reoptimized (with core atoms frozen in **TS1**). Note that in this case, the water was removed totally from the structure, and not merely moved to the MM part. The removal increases the already moderately high barrier from 19.7 to 22.0 kcal/mol, showing that the water has a lowering effect of barrier(s) in the reaction. The spin distribution of H_4B at **1a** is also slightly different, now down to −0.21 from −0.31 (Figure S17 in the Supporting Information). Hence, the water seems to help the initial partial electron transfer from H_4B to the heme, thereby lowering the barrier for the O−OH bond breakage. Still, the relatively minor changes may indicate that perhaps its bigger role is to shuffle protons in from outside the active site.[37,39]

Discussion

Three different possible reaction mechanisms for the NOS first half-reaction have been investigated by QM/MM, and only the one that proceeds via the $Por^{+\bullet}Fe^{III}$—OOH pathway was found to hydroxylate arginine in a competent mechanism that is energetically reasonable and at the same time offering a chemically logical role of the cofactor in the various steps. Scheme 4 shows the mechanistic details in a qualitative fashion. The scheme neglects the delocalization of the radical and assigns it to whichever part of the system that is the carrier of more spin density in the calculations. This should be understood in the context that the spin delocalization within the system is very large at times (Table 1). The corresponding energetics of the pathway is shown in Figure 9.

Thus, as shown in Scheme 4, the reaction starts by O−O breakage of the $Por^{+\bullet}Fe^{III}$—OOH species (**1**) and formation of an OH species (**2**) that abstracts a proton from arginine to form cpd I and the deprotonated substrate in **3**. What facilitates this stepwise process is the PCET event; the electron is transferred from the H_4B cofactor and converts the nascent OH species into a hydroxide anion, which readily abstracts a proton from the arginine substrate. Except for the PCET aspect and its drastic energy lowering effect, this step is reminiscent of the "somersault" mechanism suggested for heme oxygenase and P450.[61,62] Subsequently, the so formed cpd I activates the C═NH double bond of the deprotonated arginine, and forms an oxygenated arginine with an O—N bond (**4**). Here the cofactor plays a role of an additional electron sink; while the cpd I attacks the double

SCHEME 4: Schematic Drawing of the Electron Flows in the Reaction

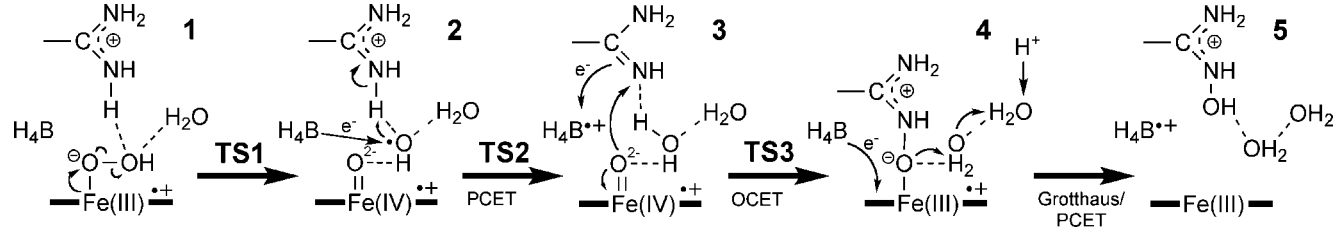

bond, $H_4B^{+\bullet}$ accepts the so formed unpaired electron from the substrate. Since this step involves oxygen transfer coupled to the electron transfer we label it as OCET in Scheme 4. Finally the second proton is shuttled to the reaction site, protonating the oxo moiety in **4** while at the same time the cofactor transfers back an electron, this time to close the porphyrin hole and form the ferric−NHA complex **5**.

The energetic features of the pathway in Figure 9 show that the rate-limiting step, not taking into account the thermal effects, is the N-oxygenation step **TS3** at 23.1 kcal/mol (18.8 with B3LYP*). The thermal effects have a considerable influence on the energy profile, most notably on **TS2** by lowering it by 9.0 kcal/mol. Hence the real rate-limiting barrier, according to the so calculated QM-only free energy, is the first step of the reaction, **TS1**, with a barrier of 17.9 kcal/mol. In addition, B3LYP* calculations indicate that both **TS1** and **TS3** may be lowered further on the order of 4 kcal/mol. Therefore, this mechanism is energetically very reasonable. Since no intermediates are observed experimentally between the iron−oxy structure and the end product, the rate-limiting step is in fact likely to be either the step via **TS1**, or the preceding step where the iron−oxy species gets protonated (of which we have no energetic information). Using the Eyring equation and available turnover rates for NOS,[4,63] one can in fact deduce an approximate value for the NOS rate-limiting (free energy) barrier. Using the fastest turnover rate value available,[63] we can estimate an absolute lower limit of NOS rate-limiting barrier to 16.4 kcal/mol, in good agreement with our value of 17.9 kcal/mol considering the exponential nature of the Eyring equation.

Taking together Scheme 4 and Figure 9, the cofactor seems to be indeed very crucial since it participates in the electron flow via PCET and OCET steps and thereby lowers the reaction barriers. Similarities exist with P450, but also differences. In $P450_{cam}$, the cpd 0 structure receives a proton from a nearby threonine to break the O−OH bond and form water. The electron needed for the water formation is taken from the a_{2u} orbital of the porphyrin, resulting in cpd I. In NOS, the species with a cpd 0 constitution is the one-electron oxidized $(H_4B\cdots Por)^{+\bullet}Fe^{III}-OOH$ species, where the oxidation equivalent is delocalized over the cofactor and the porphyrin. Here, as the O−O bond cleavage proceeds initially homolytically, the electron needed to complete the water formation step is drawn from the cofactor H_4B and the porphyrin jointly, while the proton is provided by the substrate. This deprotonation is much easier than H-atom abstraction from the arginine and at the same time, it serves to activate the substrate toward attack from cpd I.

Comparisons to Other Studies. Having discussed the most feasible mechanism for the first half-reaction, we turn to address the compatibility of this mechanism to the experimental data mentioned in the Introduction.

Source of Protons. Our mechanism in Scheme 4 shows that one proton must be provided externally. However, the second proton is provided by the arginine substrate. This crucial mechanistic feature matches the experimental conclusion derived by the cryogenic follow-up of arginine hydroxylation.[32]

Radical Formation of H_4B. Our calculations show that an extra electron is essential for the reaction to proceed past **TS2**. This electron comes from H_4B if available, but our calculations on the $Fe^{III}-OO^{2-}$ structure **0b** show that this necessary electron can also be provided by other sources, e.g., the reductase (with a loss of efficiency) or irradiation, as found experimentally.[18,32,64] Therefore, the proposed notion that H_4B is needed to supply the electron "in a timely manner" seems to be a very reasonable assumption.[18]

Reviewing the theoretical literature, two different ways of achieving an electron transfer to the iron−oxy moiety can be envisaged. One is to deprotonate H_4B,[28,29] while the other option is to protonate Fe−OO.[27] Both ways will increase the electron affinity of Fe−OO relative to H_4B, and an electron transfer may occur. We have chosen the latter strategy, consistent with the actual observation of a cationic $H_4B^{+\bullet}$ radical,[25,30] which should not have been visible if the radical transfer occurs only after deprotonation of H_4B. In addition, our previous calculations did not confirm the existence of any local minima with N3 deprotonated by the carboxylate group of the heme.[27] Hence, we conclude that H_4B deprotonation is unnecessary and a stable cation radical can be formed with the normal H_4B, if a proton is available at the iron−oxy site. However, without further specific calculations we do not categorically rule out a proton transfer from H_4B to the heme, particularly concerning deprotonation from the N5-site.

Revisiting H_4B analogue experiments where the known NOS inhibitor 4-amino-H_4B was used, our calculations support the observation that if 4-amino-H_4B would bind as a cation with the N3 site protonated (i.e., as 4-amino-H_5B^+), no electron transfer occurs and the barrier at **TS2** becomes prohibitively high due to the missing electron, akin to the case when we put H_4B in the MM region. The very same scenario has been extensively discussed before[24] as the X-ray structure clearly show that the N3 position of 4-amino-H_4B is in a clear hydrogen bonding distance to the heme propionate group. While our calculations show that this distance is largely kept even without an N3 proton (Figure S27 in the Supporting Information), the proximity of the propionate group may increase the N3 pK_a even further and a protonation there is certainly not unlikely.

Cryo-Annealing Experiments. The reason why cpd 0 is not detected in cryo-annealing experiments[32] may simply be because it is unstable, according to the reaction mechanism laid out in Scheme 4. The electronic configuration of **1** is one electron deficient (i.e., there is a porphyrin hole) compared to cpd 0, and because it is in a singlet state, it should therefore be EPR silent.

Peroxide-Shunt Pathways. Most likely, the $Fe^{III}-H_2O_2$ complex formed will undergo uncoupling favorably over other processes (as has been observed for such species),[65,66] since the bond dissociation energy of $Fe-H_2O_2$ is negative in the septet ground state. In addition, in other spin states, the cpd I formation

barrier may also be competitive with the heme oxygenase mechanism recently published.[12] Still, the $Fe^{III}-H_2O_2$ route as investigated here has a relevance to peroxide shunt pathways. In the present study we show that the cpd I species generated via $Fe^{III}-H_2O_2$ will not be able to react efficiently with a fully protonated substrate due to high barriers for the deprotonation/N-oxygenation of the substrate, consistent with a proposed "mismatch" in this reaction between cpd I and the substrate.[17] However, there is also evidence that H_2O_2 can sluggishly support the first half-reaction with a small yield of products,[18,64] detectable only with a high concentration of substrate. This result can be rationalized if one assumes that at large substrate concentrations there are non-negligible amounts of already deprotonated arginine. If so, then we have the same situation as in **3**, and the reaction can proceed over **TS3** to **4** and **5** as described above.

Substrate Arginine, Trp188, and Crystal Water Interactions. Our results show that arginine has a hydrogen bond to one or both of the oxygen atoms of the bound O_2 (Figure 4), confirming experimental results showing O_2 interaction with the substrate.[15,33−37,67] On the basis of resonance Raman study of substrate interaction with the iron−oxy species, a NOS reaction mechanism was proposed that is, in essence, the same as what we present in the current study.[15] Similarly, the crystal water is also hydrogen bonded to O_2, and seems to have a slightly lowering effect of the barriers (see the Results section). The same conclusion is also drawn for Trp188, which is hydrogen bonded to the heme cysteine sulfur, although a full in silico mutation has not been done.

Elusiveness of cpd I. While it is generally accepted that cpd I might exist in the NOS reaction mechanism, evidence for this has been scarce generating some healthy skepticism regarding this issue. In our study, cpd I exists only in energies 9.2 kcal/mol (or more) higher up than the starting point. Thus, the structure would prefer to either go back in the reaction to the more stable species **1a/b**, or forward in the reaction toward **4**, which may explain its fast reactivity and elusiveness.

Comparison to Our Previous Study.[27] The present study with a larger QM region reconfirms that cpd I formation via the doubly protonated pathway is *exothermic* by ∼25 kcal/mol (Table S1 in the Supporting Information), while in the singly protonated pathway, this is *endothermic* by ∼10 kcal/mol, with deviations within expected error margins.[13,14,56,68−70] However, the preferred thermodynamics of cpd I formation, via the double protonation path, does not really foretell whether this cpd I would be reactive toward the arginine substrate. In fact, as we showed above, the cpd I species generated in the double protonation pathway is unreactive, whereas the single protonation path is more productive toward arginine hydroxylation, even though it forms cpd I in an endothermic step. A more comprehensive discussion of the differences is outlined in the Supporting Information.

Compound II Formation in NOS. At a very late stage of the revision process of this manuscript, a DFT study on the NOS first half-reaction was published,[71] using a small gas-phase model devoid of the cofactor H_4B (assumed to be in its radical form) and consisting of substrate arginine and porphine. The authors concluded that the substrate has to be deprotonated during the O−O bond breaking process in order for the oxidizing agent to hydroxylate it, in perfect agreement with our results (conf. structure **3**). However, they also assumed that the deprotonation is done by an $Fe-OO^{2-}$ species (i.e., structure **0b**), which cannot be formed according to our QM/MM study. Furthermore, they found that, after deprotonation, the so formed neutral arginine (Arg) lost one electron to cpd I, and formed the one-electron reduced species compound II (cpd II, and $Arg^{+\bullet}$), which then abstracted a proton from $Arg^{+\bullet}$ and followed by rebound to complete the first half-reaction. By contrast, in the QM/MM study here and before,[27] Arg does not transfer an electron to cpd I and the system remains cpd I + Arg. To further test the interesting proposal of cpd II formation, we took structure **3**, which is similar to the QM model used in ref 71 but having in addition the $H_4B^{+\bullet}$ cofactor. A single point calculation without point charges (i.e., gas-phase calculation) on this structure revealed that Arg and H_4B orbitals combine to form two new orbitals, both delocalized over the Arg and H_4B moieties. One of these orbitals is singly occupied, giving rise to half a radical each on Arg and H_4B (in the protein, this half/half-delocalization shifts to about 0.2/0.8, whereby we have a "neutral" Arg; see Table 1). The other orbital is doubly occupied, because its energy level is below the a_{2u} orbital, and this prevents therefore the electron transfer from Arg to cpd I. Hence the recently reported cpd II formation,[71] which would lead to the conclusion that the $H_4B^{\bullet+}$ cation-radical would coexist with an $Arg^{\bullet+}$ cation-radical in the native system, is most likely an outcome of not including $H_4B^{\bullet+}$ in the model calculations. Thus, the cpd II-based mechanism does not occur in the wild type enzyme. However, this mechanism is fully compatible with the cryogenic experiments[32] where the extra electron is supplied by γ-irradiation and not by H_4B. As described by the authors,[71] the so generated $Fe-OO^{2-}$ species could deprotonate the substrate (as shown in **0b**). Since the H_4B analogue used in the cryogenic experiment is inactive, then in the absence of the $H_4B^{\bullet+}$ cation-radical, a cpd II species may therefore form and hydroxylate the substrate. This alternative pathway may therefore be operational whenever other electron donors, such as the reductase domain, provide the electron needed instead of H_4B.

Outlook into the Second Half-Reaction. As the second half-reaction of NOS does not have any known enzymatic precedent to date, there is a considerable interest in this reaction mechanism as well. Our results, on the first half-reaction, enable us to make some testable proposals regarding the second half-reaction. Thus, starting with Scheme 4 and replacing the substrate arginine with NHA, the same mechanism as in the first half-reaction can in principle transpire. The novel feature in this mechanism compared to most other proposals is the use of an external proton even in the second half-reaction (i.e., starting with the $Por^{+\bullet}Fe^{III}-OOH$ species and neutral H_4B, and thus requiring only one electron from the reductase for the second half-reaction). This mechanism would be consistent with several of existing experiments[18,23,72] and offer an attractive uniform reaction mechanism of NOS both half-reactions.

Conclusions

The first half-reaction of NOS exhibits an interplay between different actors, in a manner that shows similarities to, but also somewhat more complexity, than the "regular" P450 hydroxylation reactions. Our calculations show that the reaction most likely proceeds after a single proton is supplied to the system. We thus predict the existence of a $Por^{+\bullet}Fe^{III}-OOH$ species with a singly occupied a_{2u} porphyrin orbital, as the species that initiates all the transformations with the help of the cofactor H_4B. In a simplified picture, an electron is supplied from the cofactor and thereby enabling the energetically favorable water formation through PCET, similar to the cpd I formation step in P450. However, in NOS the hydroxylation of the substrate may occur through direct N-oxygenation of the substrate by cpd I,

rather than through the sequence of a hydrogen abstraction followed by a radical rebound. We can also confirm by the calculations that cpd I is nonreactive against a fully protonated substrate (the reason why peroxide-shunt reactions do not yield products) and the key role of H_4B. The cofactor H_4B turns out to be a key player in the mechanism acting alternatively as electron donor (when neutral) and an electron sink (when in its cation-radical state), and thereby providing the electron transfer component in the various coupled proton and oxygen transfer steps. These results for the first half-reaction mechanism enable us to propose a similar mechanism for the second half-reaction.

Acknowledgment. This paper is dedicated to Robert B. Gerber towards his forthcoming 65th birthday. The research is supported by an ISF grant to S.S. (ISF 16/06), and M.A.C. is supported by Generalitat de Catalunya.

Supporting Information Available: Evaluation of the use of B3LYP and B3LYP/MM in heme systems, as well as a comprehensive comparison to the previous study.[27] Spin distribution, energies, and geometries of all the structures in this study. This material is available free of charge via the Internet at http://pubs.acs.org.

References and Notes

(1) Garthwaite, J.; Boulton, C. L. *Annu. Rev. Physiol.* **1995**, *57*, 683.
(2) Kerwin, J. F. J.; Lancaster, J. R. J.; Feldman, P. L. *J. Med. Chem.* **1995**, *38*, 4343.
(3) MacMicking, J.; Xie, Q. W.; Nathan, C. *Annu. Rev. Immunol.* **1997**, *15*, 323.
(4) Stuehr, D. J.; Griffith, O. W. In *Advances in Enzymology Related Areas of Molecular Biology*; Meister, A., Ed.; Interscience: New York, 1992; Vol. 65, p 287.
(5) Stuehr, D. J. *Biochim. Biophys. Acta* **1999**, *1411*, 217.
(6) Stuehr, D. J.; Santolini, J.; Wang, Z. Q.; Wei, C. C.; Adak, S. *J. Biol. Chem.* **2004**, *279*, 36167.
(7) Groves, J. T.; Wang, C. C.-Y. *Curr. Opin. Chem. Biol.* **2000**, *4*, 687.
(8) Rosen, G. M.; Tsai, P.; Pou, S. *Chem. Rev.* **2002**, *102*, 1191.
(9) Stuehr, D. J.; Pou, S.; Rosen, G. M. *J. Biol. Chem.* **2001**, *276*, 14533.
(10) Shaik, S.; Kumar, D.; de Visser, S. P.; Altun, A.; Thiel, W. *Chem. Rev.* **2005**, *105*, 2279.
(11) Chen, H.; Hirao, H.; Derat, E.; Schlichting, I.; Shaik, S. *J. Phys. Chem. B* **2008**, *112*, 9490.
(12) Chen, H.; Moreau, Y.; Derat, E.; Shaik, S. *J. Am. Chem. Soc.* **2008**, *130*, 1953.
(13) Senn, H. M.; Thiel, W. In *Topics in Current Chemistry*; Reiher, M., Ed.; Springer-Verlag: Berlin/Heidelberg, 2007; Vol. 268, p 173.
(14) Lin, H.; Truhlar, D. G. *Theor. Chem. Acc.* **2007**, *117*, 185.
(15) Li, D.; Kabir, M.; Stuehr, D. J.; Rousseau, D. L.; Yeh, S.-R. *J. Am. Chem. Soc.* **2007**, *129*, 6943.
(16) Pufahl, R. A.; Wishnok, J. S.; Marletta, M. A. *Biochemistry* **1995**, *34*, 1930.
(17) Zhu, Y.; Silverman, R. B. *Biochemistry* **2008**, *47*, 2231.
(18) Adak, S.; Wang, Q.; Stuehr, D. J. *J. Biol. Chem.* **2000**, *275*, 33554.
(19) Hurshman, A. R.; Marletta, M. A. *Biochemistry* **2002**, *41*, 3439.
(20) Hurshman, A. R.; Krebs, C.; Edmondson, D. E.; Huynh, B. H.; Marletta, M. A. *Biochemistry* **1999**, *38*, 15689.
(21) Bec, N.; Gorren, A. F. C.; Mayer, B.; Schmidt, P. P.; Andersson, K. K.; Lange, R. *J. Inorg. Biochem.* **2000**, *81*, 207.
(22) Wei, C. C.; Wang, Z. Q.; Wang, Q.; Meade, A. L.; Hemann, C.; Hille, R.; Stuehr, D. J. *J. Biol. Chem.* **2001**, *276*, 315.
(23) Wei, C. C.; Wang, Z. Q.; Hemann, C.; Hille, R.; Stuehr, D. J. *J. Biol. Chem.* **2003**, *278*, 46668.
(24) Crane, B. R.; Arvai, A. S.; Ghosh, S.; Getzoff, E. D.; Stuehr, D. J.; Tainer, J. A. *Biochemistry* **2000**, *39*, 4608.
(25) Sørlie, M.; Gorren, A. C. F.; Marchal, S.; Shimizu, T.; Lange, R.; Andersson, K. K.; Mayer, B. *J. Biol. Chem.* **2003**, *278*, 48602.
(26) Hurshman, A. R.; Krebs, C.; Edmondson, D. E.; Marletta, M. A. *Biochemistry* **2003**, *42*, 13287.
(27) Cho, K.-B.; Derat, E.; Shaik, S. *J. Am. Chem. Soc.* **2007**, *129*, 3182.
(28) Morao, I.; Periyasamy, G.; Hillier, I. H.; Joule, J. A. *Chem. Commun.* **2006**, 3525–3527.
(29) Menyhárd, D. K. *Chem. Phys. Lett.* **2004**, *392*, 439.
(30) Schmidt, P. P.; Lange, R.; Gorren, A. C. F.; Werner, E. R.; Mayer, B.; Andersson, K. K. *J. Biol. Inorg. Chem.* **2004**, *6*, 151.
(31) Raman, C. S.; Li, H.; Martásek, P.; Král, V.; Masters, B. S. S.; Poulos, T. L. *Cell* **1998**, *95*, 939.
(32) Davydov, R.; Ledbetter-Rogers, A.; Martásek, P.; Larukhin, M.; Sono, M.; Dawson, J. H.; Masters, B. S. S.; Hoffman, B. M. *Biochemistry* **2002**, *41*, 10375.
(33) Berka, V.; Wang, L.-H.; Tsai, A.-L. *Biochemistry* **2008**, *47*, 405.
(34) Berka, V.; Yeh, H.-C.; Gao, D.; Kiran, F.; Tsai, A.-L. *Biochemistry* **2004**, *43*, 13137.
(35) Chartier, F. J. M.; Blais, S. P.; Couture, M. *J. Biol. Chem.* **2006**, *281*, 9953.
(36) Chartier, F. J. M.; Couture, M. *J. Biol. Chem.* **2007**, *282*, 20877.
(37) Li, H.; Igarashi, J.; Jamal, J.; Wang, W.; Poulos, T. L. *J. Biol. Inorg. Chem.* **2006**, *11*, 753.
(38) Fedorov, R.; Ghosh, D. K.; Schlichting, I. *Arch. Biochem. Biophys.* **2003**, *409*, 25.
(39) Martin, N. I.; Woodward, J. J.; Winter, M. B.; Beeson, W. T.; Marletta, M. A. *J. Am. Chem. Soc.* **2007**, *129*, 12563.
(40) Yoshioka, S.; Takahashi, S.; K., I.; Morishima, I. *J. Inorg. Biochem* **2000**, *81*, 141.
(41) Ogliaro, F.; de Visser, S. P.; Shaik, S. *J. Inorg. Biochem.* **2002**, *91*, 554.
(42) Adak, S.; Crooks, C.; Wang, Q.; Crane, B. R.; Tainer, J. A.; Getzoff, E. D.; Stuehr, D. J. *J. Biol. Chem.* **1999**, *274*, 26907.
(43) Adak, S.; Wang, Q.; Stuehr, D. J. *J. Biol. Chem.* **2000**, *275*, 17434.
(44) Poulos, T. L. *Nat. Prod. Rep.* **2007**, *24*, 504.
(45) Kohn, W.; Sham, L. J. *Phys. Rev.* **1965**, *A140*, 1133.
(46) Rosenthal, J.; Nocera, D. G. *Acc. Chem. Res.* **2007**, *40*, 543.
(47) Crane, B. R.; Arvai, A. S.; Ghosh, D. K.; Wu, C.; Getzoff, E. D.; Stuehr, D. J.; Tainer, J. A. *Science* **1998**, *279*, 2121.
(48) Sherwood, P.; de Vries, A. H.; Guest, M. F.; Schreckenbach, G.; Catlow, C. R. A.; French, S. A.; Sokol, A. A.; Bromley, S. T.; Thiel, W.; Turner, A. J.; Billeter, S.; Terstegen, F.; Thiel, S.; Kendrick, J.; Rogers, S. C.; Casci, J.; Watson, M.; King, F.; Karlsen, E.; Sjøvoll, M.; Fahmi, A.; Schäfer, A.; Lennartz, C. J. *J. Mol. Struct. (THEOCHEM)* **2003**, *632*, 1.
(49) Ahlrichs, R.; Bär, M.; Häser, M.; Horn, H.; Kölmel, C. *Chem. Phys. Lett.* **1989**, *162*, 165.
(50) Becke, A. D. *Phys. Rev. A* **1988**, *38*, 3098.
(51) Becke, A. D. *J. Chem. Phys.* **1993**, *98*, 1372.
(52) Becke, A. D. *J. Chem. Phys.* **1993**, *98*, 5648.
(53) Lee, C.; Yang, W.; Parr, R. G. *Phys. Rev. B* **1988**, *37*, 785.
(54) *Jaguar 5.5*, Schrodinger, L.L.C.: Portland, Oregon, 2003.
(55) Reiher, M.; Salomon, O.; Hess, B. A. *Theor. Chem. Acc.* **2001**, *107*, 48.
(56) Siegbahn, P. E. M. *J. Biol. Inorg. Chem.* **2006**, *11*, 695.
(57) MacKerell, A. D.; Bashford, D.; Bellott, M.; Dunbrack, R. L.; Evanseck, J. D.; Field, M. J.; Fischer, S.; Gao, J.; Guo, H.; Ha, S.; Joseph-McCarthy, D.; Kuchnir, L.; Kuczera, K.; Lau, F. T. K.; Mattos, C.; Michnick, S.; Ngo, T.; Nguyen, D. T.; Prodhom, B.; Reiher, W. E.; Roux, B.; Schlenkrich, M.; Smith, J. C.; Stote, R.; Straub, J.; Watanabe, M.; Wiorkiewicz-Kuczera, J.; Yin, D.; Karplus, M. *J. Phys. Chem. B* **1998**, *102*, 3586.
(58) Bakowies, D.; Thiel, W. *J. Phys. Chem.* **1996**, *100*, 10580.
(59) Kästner, J.; Senn, H. M.; Thiel, S.; Otte, N.; Thiel, W. *J. Chem. Theory Comput.* **2006**, *2*, 452.
(60) de Visser, S. P.; Ogliaro, F.; Harris, N.; Shaik, S. *J. Am. Chem. Soc.* **2001**, *123*, 3037.
(61) Sharma, P. K.; Kevorkiants, R.; de Visser, S. P.; Kumar, D.; Shaik, S. *Angew. Chem., Int. Ed.* **2004**, *43*, 1129.
(62) Bach, R. D.; Dmitrenko, O. *J. Am. Chem. Soc.* **2006**, *128*, 1474.
(63) Stuehr, D. J.; Cho, H. J.; Kwon, N. S.; Weise, M. F.; Nathan, C. F. *Proc. Natl. Acad. Sci. U.S.A.* **1991**, *88*, 7773.
(64) Adhikari, S.; Ray, S.; Gachhui, R. *FEBS Lett.* **2000**, *475*, 35.
(65) Heinzel, B.; John, M.; Klatt, P.; Bohme, E.; Mayer, B. *Biochem. J.* **1992**, *281*, 627.
(66) Rosen, G. M.; Tsai, P.; Weaver, J.; Porasuphatana, S.; Roman, L. J.; Starkov, A. A.; Fiskum, G.; Pou, S. *J. Biol. Chem.* **2002**, *277*, 40275.
(67) Li, H.; Raman, C. S.; Martasek, P.; Masters, B. S. S.; Poulos, T. L. *Biochemistry* **2001**, *40*, 5399.
(68) Neese, F. *Inorg. Chim. Acta* **2002**, *337*, 181.
(69) Altun, A.; Shaik, S.; Thiel, W. *J. Comput. Chem.* **2006**, *27*, 1324.
(70) Zheng, J.; Altun, A.; Thiel, W. *J. Comput. Chem.* **2007**, *28*, 2147.
(71) de Visser, S. P.; Tan, L. S. *J. Am. Chem. Soc.* **2008**, *130*, 12961.
(72) Huang, H.; Hah, J.-M.; Silverman, R. B. *J. Am. Chem. Soc.* **2001**, *123*, 2674.

JP8073199